

Perfusion Imaging

Magnetic Resonance Imaging of Myocardial Perfusion in Single-Vessel Coronary Artery Disease: Implications for Transmural Assessment of Myocardial Perfusion

Jan T. Keijer,^{1,3,4} Albert C. van Rossum,^{1,3,4} Norbert Wilke,²
Machiel J. van Eenige,^{1,3,4} Michael Jerosch-Herold,² Jean G.F.
Bronzwaer,^{1,3,4} and Cees A. Visser^{1,3,4}

¹Department of Cardiology, Free University Hospital, Amsterdam, The Netherlands

²University of Minnesota Center for MR Research

³Interuniversity Cardiology Institute (ICIN), Utrecht, The Netherlands

⁴Institute for Cardiovascular Research Free University (ICARVU), Amsterdam, The Netherlands

ABSTRACT

The purpose of the study was to investigate the potential of magnetic resonance imaging (MRI) to assess transmural differences in myocardial perfusion. Contrast-enhanced MRI was performed at rest and during hyperemia in a dog model and in 22 patients with single-vessel coronary artery disease. From MR signal intensity-versus-time curves, three perfusion parameters were derived: maximum myocardial contrast enhancement (MCE), slope, and inverse mean transit time (1/MTT). In dogs, MCE correlated well ($r = 0.87$, $p < 0.00001$) with microsphere-assessed myocardial blood flow. In the patients, the subendocardial MCE decreased during hyperemia (0.89 ± 0.18 vs. 0.74 ± 0.15 , $p < 0.003$) and was lower in subendocardium than in subepicardium (0.74 ± 0.15 vs. 0.84 ± 0.21 , $p < 0.02$). Parameters slope and 1/MTT paralleled MCE. Contrast-enhanced MRI reflects the transmural redistribution of myocardial perfusion during hyperemia. Perfusion abnormalities can be identified most distinctly in subendocardial myocardium.

KEY WORDS: Gadolinium-DTPA; Magnetic resonance imaging; Myocardial perfusion.

INTRODUCTION

Although coronary angiography (CAG) is the current gold standard in the management of patients with coronary artery disease (CAD), the anatomic severity of a coronary artery stenosis is not always an adequate indicator

of its functional consequences on myocardial perfusion (1,2). Therefore, perfusion imaging techniques are often used to obtain additional information on myocardial perfusion.

²⁰¹Thallium- and ^{99m}technetium-scintigraphy have proven their clinical value but are limited by their spatial

Received September 9, 1999; Accepted February 24, 2000

Address reprint requests to J.T. Keijer.

resolution and relatively low specificity (3,4). Positron emission tomography has better spatial resolution and allows quantification of myocardial perfusion (5). The availability of this technique for routine clinical use, however, is limited.

Magnetic resonance imaging (MRI) allows evaluation of myocardial perfusion with relatively high spatial and temporal resolution (6–8). Fast MRI techniques (9,10) allow imaging the first-pass of an MR contrast agent (11) after bolus injection. These techniques have been shown to visualize abnormalities in myocardial perfusion (12–18) and enable derivation of perfusion-related parameters such as maximum contrast enhancement and slope of the wash-in curve of the contrast agent. Abnormalities in these parameters have been reported in patients with myocardial infarction and patients with a >90% coronary artery stenosis at rest and during dipyridamole stress (12–18).

Kinetic modeling provides more quantitative estimates of myocardial perfusion (19–23). For example, indicator dilution theory (24) describes the relation between myocardial blood flow (F), volume (V), and the mean transit time (MTT) of the contrast agent through the myocardium, according to the equation $1/MTT = F/V$. This relation between $1/MTT$ and myocardial blood flow was previously confirmed in an experimental MRI study (25). We previously showed methodologic requirements for the first-pass MRI approach in humans (26) and demonstrated the agreement of first-pass MRI and ²⁰¹thallium single photon emission computed tomography in patients with single-vessel CAD and in patients with myocardial infarction (17,18).

The first manifestations of myocardial hypoperfusion caused by a coronary stenosis predominantly occur in the subendocardial layer of the myocardium (27,28). Therefore, the detection of CAD might be enhanced if MRI allowed imaging of differences in transmural myocardial perfusion.

The aim of the present study was to investigate the feasibility of quantification of myocardial perfusion parameters and to localize perfusion abnormalities in three circumferential layers of the myocardium in a dog model and in patients with single-vessel CAD.

METHODS

Dog Studies

Animal studies were carried out at the University of Minnesota with protocols adhering to the guidelines established in *Position of the American Heart Association on Research Animal Use*. Three dogs were surgically in-

strumented as described elsewhere (25) by inserting catheters in the left ventricle and ascending aorta (for pressure monitoring), the left atrium (for injection of microspheres and MR contrast agent), and the femoral vein (for administration of dipyridamole). Partial occlusions were induced by a hydraulic occluder placed around the left anterior descending (LAD) coronary artery proximal to a Doppler flowmeter used for verification of the intervention. Microspheres for blood flow measurements were injected to validate retrospectively the severity of the occlusions. Microsphere injection protocol and blood flow calculations were performed as previously described (25).

Dipyridamole was administered intravenously (0.8 mg/kg) for a period of 2 min to create maximum coronary dilatation. Two to 4 min later, a bolus of gadolinium-DTPA (Gd-DTPA, Schering AG Germany, 0.05 mmol/kg) was injected into the left atrium, during the maximum vasodilatory state. Nine first-pass MRI acquisitions were performed in three dogs at basal, midventricular, and apical short-axis planes. Imaging was performed under various conditions. In dog 1, imaging was done during dipyridamole, without stenosis. In dog 2, imaging was also done during dipyridamole. The occluder was inflated until a moderate stenosis was induced at an intracoronary pressure of 65 mm Hg. In dog 3, imaging was done at rest after introduction of a severe stenosis (intracoronary pressure, 35 mm Hg). After completion of the microsphere and MRI protocol, dogs were killed and their hearts excised for subsequent microsphere flow analysis.

Patients

The study population consisted of 22 patients (17 men and 5 women, aged 56 ± 11 yr, range 32–76 yr) with chest pain. All patients gave their informed consent for participation in the study, according to the ethical standards of the committee on human research of the Free University Hospital. Patients were referred for diagnostic cardiac catheterization after either a previous positive exercise test or an episode of unstable angina with subsequent hospital admission. At CAG, all patients had significant single-vessel CAD (>70% luminal diameter stenosis). The stenosis location was the LAD in 13 patients, the left circumflex (LCx) in 2, and the right coronary artery (RCA) in 7 patients. All had normal left ventricular volumes and systolic function as assessed by left ventriculography or routine echocardiography. Patients were all in sinus rhythm and had no valvular heart disease, diabetes mellitus, left ventricular hypertrophy or

pathologic Q waves on electrocardiogram (ECG), or other clinical evidence of previous myocardial infarction. The clinical characteristics of the patient group are listed in Table 1. Nitrates and calcium antagonists were discontinued 24 hr before the MR study. Patients were requested to refrain from consuming xanthine-containing foods and beverages in the 24 hr before the MR study. Eleven patients underwent additional quantitative CAG 2 hr after the MRI protocol.

MRI Protocol

In the patients, a 6-French intravenous catheter (Cordis, Roden, The Netherlands) was introduced toward the right atrium. In patients 1 to 11, this was achieved through an antecubital vein, and right atrial position was checked by intracardiac ECG electrode or estimated from remaining catheter length. In patients 12 to 22, the catheter was introduced via the right femoral vein and right atrial position was verified by fluoroscopy. Breathholding was practiced before the MR study. MR acquisition was

done on either a 1.5-T system (dogs and patients 1 to 11, Siemens AG, Erlangen, Germany) with a Helmholtz coil or a 1.0-T system (patients 12 to 22, Siemens) with quadruple phased array coil, within 4 weeks of cardiac catheterization. A double-oblique short-axis plane (slice thickness, 10 mm) was imaged at the midpapillary muscle level because it represents all perfusion territories of the three major coronary arteries. The inversion time (TI) was adjusted to null the signal from the myocardium (TI, 75–175 msec). A turbo-fast low-angle single-shot sequence (8) with a 180-degree inversion pulse was applied (TR 4.8 msec, TE 2 msec, excitation angle 10 degrees, field of view 250² or 300² mm², matrix size 90 × 128), resulting in an in-plane resolution of approximately 3 × 2 mm². Forty-five ECG-triggered images were obtained in supine position (one every heartbeat) during breathholding. A bolus of 0.03 mmol/kg of Gd-DTPA was injected with a hand injector at the fifth heartbeat after the start of imaging to allow imaging of a steady-state baseline situation. First-pass images were acquired before and after intravenous dipyridamole (0.56 mg/kg, ad-

Table 1

Clinical Characteristics

Patient	Age (yr)/Sex	Affected Vessel (visual % diameter stenosis of CAG)	X-ECG	Minimal Luminal Stenosis Area (QCA)
1	45 M	RCA 90–99	n.a.	n.a.
2	63 M	RCA 90–99	+	n.a.
3	69 M	LAD 70–90	n.a.	n.a.
4	67 F	LCx 70–90	+	n.a.
5	32 M	LAD 90–99	+	n.a.
6	44 M	LAD 90–99	+	n.a.
7	76 F	LAD 90–99	n.a.	n.a.
8	51 F	LAD 90–99	+	n.a.
9	59 M	LAD 70–90	+	n.a.
10	36 M	RCA 90–99	–	n.a.
11	59 M	LAD 90–99	+	n.a.
12	51 M	LAD 99	n.a.	79
13	50 M	LAD 90–99	+	98
14	51 M	LAD 90–99	+	95
15	69 M	RCA 99	–	99
16	56 M	LCx 99	+	89
17	61 F	LAD 90–99	+	89
18	55 M	RCA 90–99	+	99
19	51 M	RCA 70–90	–	95
20	59 M	LcX 90–99	–	65
21	73 F	RCA 70–90	+	87
22	51 M	LAD 70–90	+	89

–/+, negative/positive test result; n.a., not available.

ministered intravenously for a period of 4 min). Before stress imaging, the myocardium was nulled again.

Flow Data Analysis

Microsphere flow values were obtained in six radial segments of the myocardium. Each segment yielded separate values for subendocardial, mesocardial, and subepicardial myocardium.

MRI Data Analysis

First-pass MR images of canine and patient studies were analyzed off-line on a workstation (SUN Microsystems, Mountain View, CA) (18). Myocardial contours were drawn on the short-axis image with maximum myocardial contrast enhancement (MCE). The contours were propagated to the other images while adjusting for occasional shifts in heart position. Using custom software, the myocardium was divided in 30 radii (of 12 degrees each) that were subdivided in three circumferential (subendocardial, mesocardial, and subepicardial) layers of equal thickness. For every Gd-DTPA injection, myocardial signal intensity (SI)-time curves were obtained.

If any extra systole was present during imaging, this was noted. During analysis, images with sudden change in SI that could not possibly be due to contrast agent were rejected from analysis. Such a beat-to-beat change could also easily be identified in the SI-time curve.

To obtain information about the input function, an additional region was drawn in the left ventricular cavity, yielding a left ventricular SI-time curve. A nonlinear, least-squares, gamma variate curve fit (29) was applied to the first circulation data points of the SI-time curves.

From each curve fit, perfusion parameters MCE, slope, and $1/MTT$ were derived. To account for differences in input function, left ventricular MTT was subtracted from the measured MTT, yielding input-corrected myocardial MTT (30). A 10-point filter was applied to smooth the effect of occasional outliers, and the perfusion parameters were displayed in a circumferential profile plot.

To match with the microsphere data (obtained from six radial segments subtending three myocardial layers each), circumferential profiles (containing 30 radii) of the canine perfusion parameters were condensed into six corresponding radial segments. This was achieved by averaging five radii. In this way, each myocardial layer could be compared separately.

In the patients, the coronary artery distribution was projected on to the short-axis myocardium according to the following classification, where 0 degrees represents

the three o'clock position and degrees are counted clockwise: LAD, 150–315 degrees; LCx, 315–360 degrees and 0–45 degrees; and RCA, 45–150 degrees. The short-axis myocardium was thus divided in normal and abnormal perfusion beds. The three contiguous regions in the center of the perfusion bed that was perfused by a stenosed vessel were defined as abnormal myocardium. Normal myocardium was defined as the three contiguous myocardial regions in the center of the normal perfusion bed.

Microsphere flow values were expressed in two ways:

1. As the flow in the abnormal perfusion bed relative to normal myocardium, the abnormal/normal (A/N) ratio. (This was also done for the acquisitions where no LAD stenosis was induced to obtain control values);
2. As the flow in the subendocardium relative to the subepicardium, the subendocardial/subepicardial (endo/epi) ratio.

MR perfusion parameters were presented accordingly.

Quantitative Coronary Angiography

CAG was performed approximately 2 hr after the completion of the MRI protocol. No premedication was given. Using hand injections of 5 to 10 ml of ionic contrast material (Hexabrix, Guerbet, The Netherlands), the stenosis in the coronary artery was visualized in at least two projections. In 11 patients, maximum stenosis severity was measured and compared with the reference diameter of the stenotic vessel (i.e., a computer-derived reconstruction of the original arterial dimensions at the site of the obstruction).

Statistical Analysis

All data are expressed as means \pm SD. A least-squares correlation technique was used in the analysis of myocardial blood flow and MR parameters in dogs. Linear regression analysis was performed in the comparison of microsphere values with MR parameters and in the comparison between quantitative angiography and MRI perfusion parameters. Differences in ratios of MR perfusion parameters were analyzed by paired Student's *t*-test.

RESULTS

Dog Studies

One hundred sixty-two segmental values of myocardial blood flow were obtained and compared with corre-

sponding MR perfusion parameters. A/N ratios of myocardial blood flow and A/N ratio of MCE correlated well (overall correlation $r = 0.87$, $p < 0.00001$; Fig. 1A), and this relation was similar in all three layers of the myocardium (Fig. 1, B–D). The overall correlations with A/N ratios of slope and $1/MTT$ were 0.74 ($p < 0.0001$) and 0.85 ($p < 0.0001$), respectively.

The ratios of subendocardial and subepicardial flow (the endo/epi ratios) were calculated and compared with the MRI parameters. Figure 2 shows the overall relation between these ratios (overall correlation $r = 0.73$, $p < 0.001$; Fig. 2A) and the separate correlations in normal myocardium ($r = 0.65$, $p = 0.056$; Fig. 2B) and in abnormal myocardium ($r = 0.93$, $p < 0.001$; Fig. 2C).

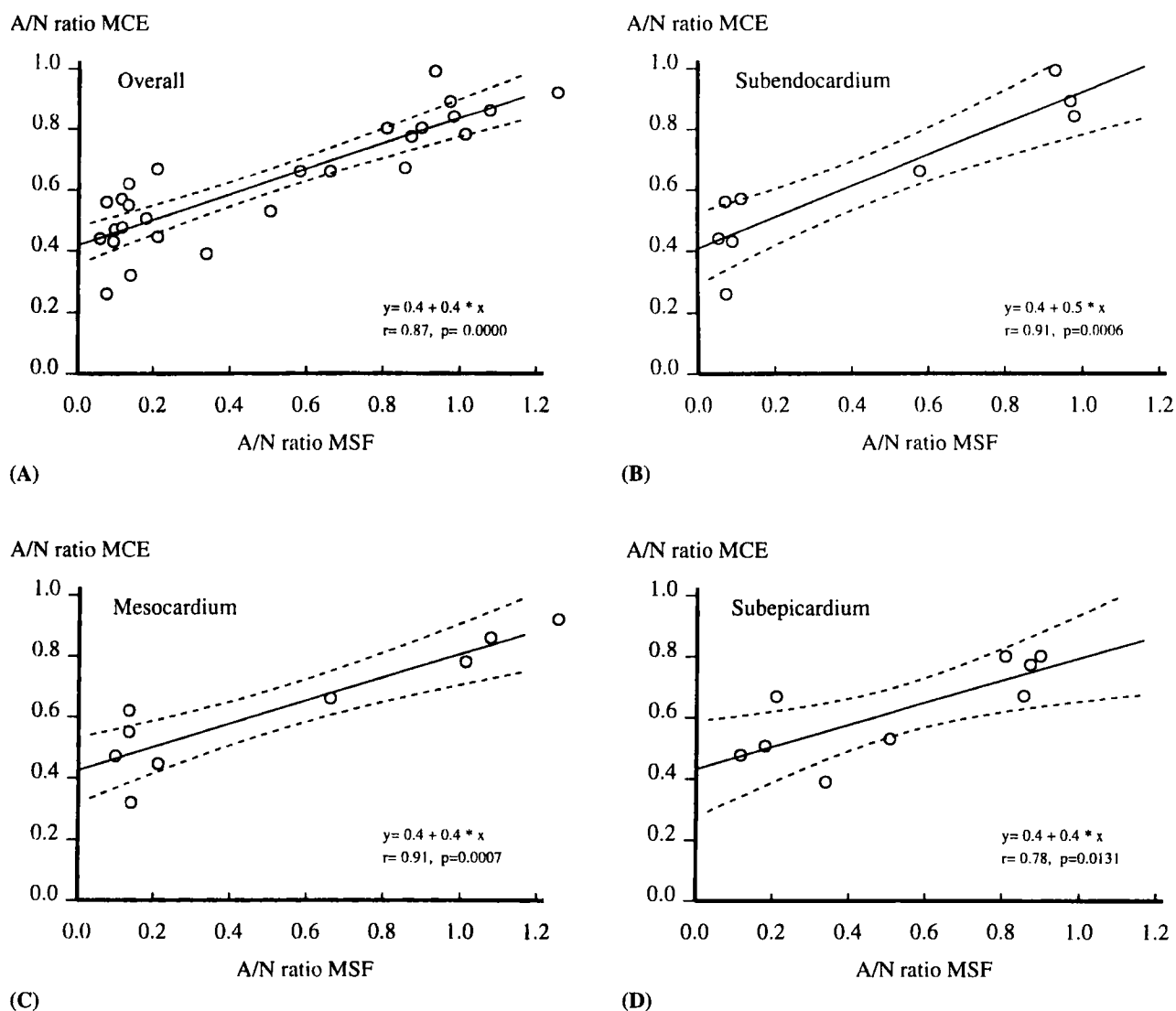
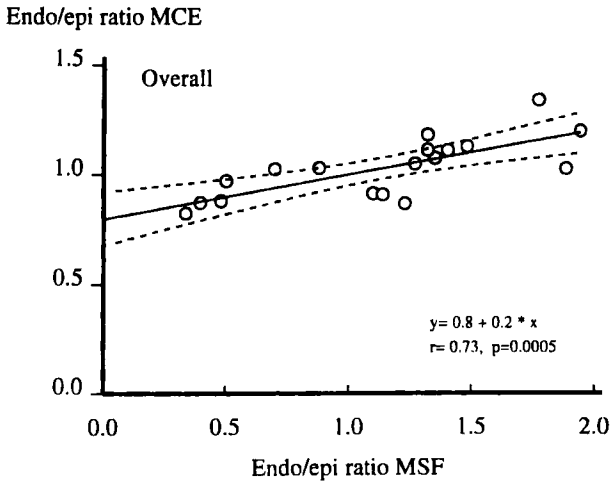
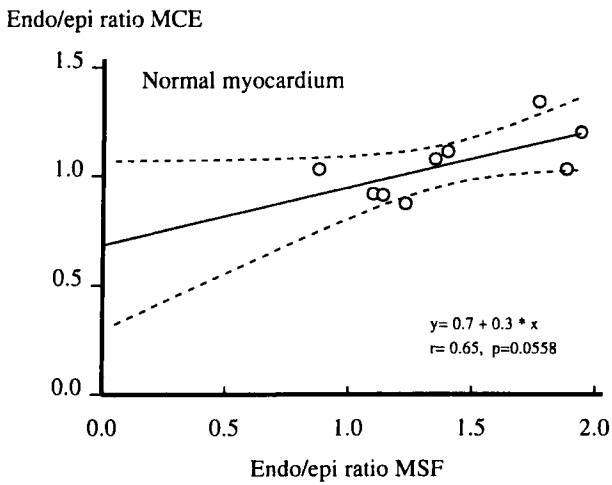


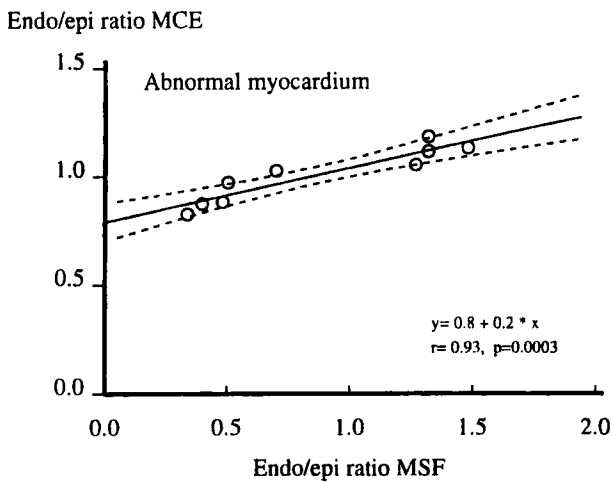
Figure 1. Relation between relative myocardial blood flow (microsphere blood flow [MSF], assessed by radiolabeled microspheres) and relative maximum MCE (assessed by MRI) in nine dog studies. The A/N ratio represents the ratio of values obtained from abnormal and normal perfusion beds, respectively. (A) Overall, (B) subendocardium (endo), (C) mesocardium (mid), and (D) subepicardium (epi). A/N ratios in controls were calculated analogous to A/N ratios in dogs with a coronary artery stenosis. Solid lines represent the correlation, and the dotted lines represent the 95% confidence intervals.



(A)



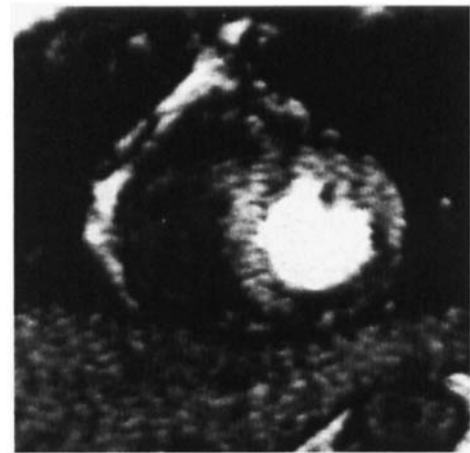
(B)



(C)



(A)



(B)

Figure 3. Example of midventricular short-axis images in a patient with a 99% RCA stenosis during maximum contrast enhancement, before (A) and after (B) dipyrindamole. After dipyrindamole, a perfusion defect is visible in the inferior wall.

Figure 2. Relation between relative myocardial blood flow (microsphere blood flow [MSF], assessed by radiolabeled microspheres) and relative maximum MCE (assessed by MRI) in the normal and abnormal canine myocardium. The endo/epi ratio represents the ratio of values obtained from endocardium and epicardium, respectively. (A) Overall, (B) normal myocardium, and (C) abnormal myocardium. Note that four data points are within normal limits, three of which result from control acquisitions where no stenosis was induced and one of which results from an acquisition in a basal slice of a dog with severe stenosis at rest. In this case, the perfusion abnormality may have been situated at a more distal level.

The overall correlation with endo/epi ratios of slope and 1/MTT was 0.67 ($p < 0.003$) and 0.79 ($p < 0.0002$), respectively.

Patient Studies

During dipyridamole, heart rate increased from 58.5 ± 10.4 to 72.4 ± 13.6 ($p < 0.001$). Mean arterial pressure was 95.4 ± 13.9 and 95.3 ± 15.3 mm Hg, respectively. Ten patients had anginal complaints during dipyridamole, which spontaneously disappeared without the need for aminophylline. Figure 3 shows an example of a perfusion defect during dipyridamole in a patient with a 90–99% diameter stenosis in the right coronary artery. The circumferential profiles of MR perfusion parameters in this patient (Fig. 4) show a dipyridamole-induced decrease in regional values of the respective MR perfusion parameters in the perfusion bed of the RCA.

Relative Values of Flow Parameters

The A/N ratio of MCE in endocardial regions at rest was 0.89 ± 0.18 and decreased during hyperemia to

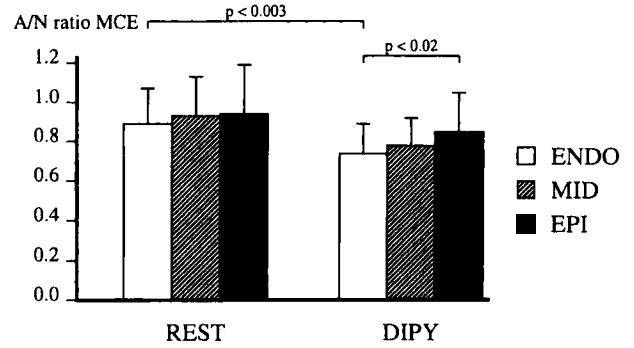


Figure 5. The A/N of MRI perfusion parameter MCE at the three transmural levels in the patient group. MCE in subendocardial myocardium decreased during dipyridamole (DIPY) and was lower than in subepicardial myocardium, indicating dipyridamole-induced subendocardial hypoperfusion.

0.74 ± 0.15 ($p < 0.003$; Fig. 5). There were no significant transmural differences in A/N ratios at rest. During dipyridamole, the A/N ratio of MCE in subendocardial myocardium was lower than in subepicardial myocardium (0.74 ± 0.15 vs. 0.84 ± 0.21 , $p < 0.02$; Fig. 5). A/N ratios of MCE, slope, and 1/MTT are listed in

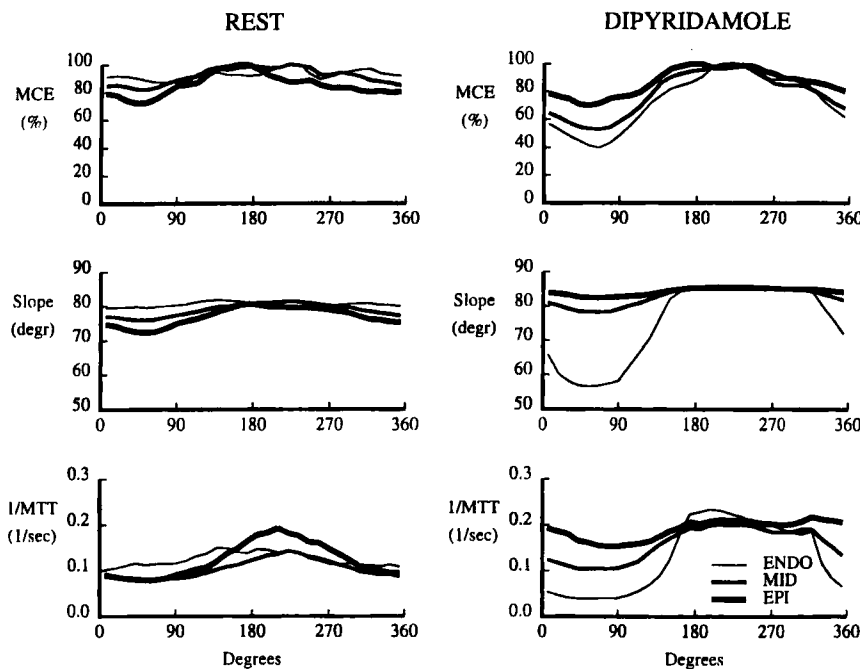


Figure 4. Example of the circumferential profiles of MCE, slope, and 1/MTT in the same as in patient Fig. 3 in the three myocardial layers, at rest and after dipyridamole. The perfusion bed of the RCA is situated between 45 and 150 degrees.

Table 2

Ratios of Perfusion Parameters in Abnormal and Normal Myocardium

A/N Ratios	Rest			Stress		
	ENDO	MID	EPI	ENDO	MID	EPI
MCE	0.89 ± 0.18	0.90 ± 0.19	0.93 ± 0.25	0.74 ± 0.15*†	0.79 ± 0.15	0.84 ± 0.21
Slope	0.84 ± 0.22	0.86 ± 0.20	0.89 ± 0.31	0.64 ± 0.18‡§	0.72 ± 0.16	0.79 ± 0.21
1/MTT	0.94 ± 0.15	0.95 ± 0.16	0.96 ± 0.20	0.80 ± 0.21 ¶	0.85 ± 0.13	0.88 ± 0.21

* $p < 0.003$ pre vs. post; † $p < 0.02$ endo vs. epi; ‡ $p < 0.002$ pre vs. post; § $p < 0.008$; || $p < 0.002$ pre vs. post; ¶ $p = 0.12$ endo vs. epi. ENDO, endocardium; MID, mesocardium; EPI, epicardium.

Table 2. Results were not different between the groups imaged at 1.0 and 1.5 T.

Transmural Distribution of Flow Parameters

Under resting conditions, the endo/epi ratio of MCE in normal myocardium was 1.25 ± 0.29 and in the abnormal myocardium, 1.18 ± 0.18 (NS). During stress, these ratios decreased to 1.08 ± 0.23 (NS, pre- vs. postdipyridamole) and 0.96 ± 0.21 , respectively ($p < 0.0002$ pre- vs. postdipyridamole, $p < 0.002$ normal vs. abnormal myocardium) (Fig. 6, Table 3).

Effect of Coronary Artery Stenosis Severity on MRI Perfusion Parameters

There was a trend between severity of coronary artery stenosis and subendocardial A/N ratio (Fig. 7A) and with endo/epi ratio in abnormal myocardium (Fig. 7B).

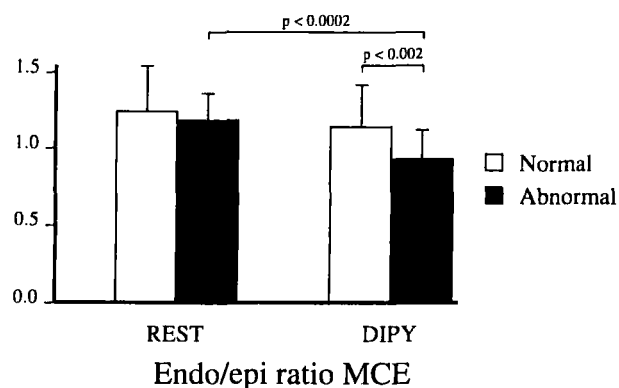


Figure 6. The transmural distribution of perfusion parameter MCE in the patient group. The decrease in endo/epi ratios of MCE reflects the redistribution of myocardial blood flow during hyperemia. The lower endo/epi ratio in abnormal myocardium reflects the impediment of blood flow in predominantly the subendocardial myocardium.

DISCUSSION

Its high spatial resolution makes MRI well suited for the study of transmural variations in myocardial perfusion. The possibility to assess transmural variations in myocardial blood flow with first-pass MRI has previously been indicated by Wilke et al. in dogs (25) and in patients (31,32). Lima et al. (33) recently described different transmural patterns in myocardial SI in patients with reperfused and nonreperfused myocardial infarction, illustrating the potential of MRI to visualize transmural differences in myocardial perfusion.

In the present study, optimal first-pass conditions (at least for a venous approach) were achieved by central injection of Gd-DTPA. This promotes compactness of the bolus, which enhances spatial differences in Gd-DTPA concentration during first-pass and limits recirculation effects, thus allowing more distinct imaging of separate first and second pass (26).

Analysis of the first-pass studies was performed on a contour-based approach, thus minimizing subjective positioning of regions of interest and enabling automated (blinded) subdivision of the myocardium in three transmural layers.

Abnormal/Normal Ratios

This study shows that in dogs, relative MCE correlates well with relative myocardial blood flow regardless of its transmural position within the myocardial wall and regardless of flow state. The presentation of relative perfusion has the advantage that it is independent of the myocardial input function. Furthermore, it largely excludes the effect of changes in vascular volume that occur due to autoregulation or pharmacologic stress (34,35). As suggested by the slope of the relation between relative myocardial blood flow and relative MCE (Fig. 1), relative MCE is proportional to changes in relative myocardial blood flow, but the relation is blunted and displays a 0.4

Table 3
Ratios of Perfusion Parameters in Subendocardium and Subepicardium

Endo/Epi Ratios	Rest		Stress	
	Abnormal	Normal	Abnormal	Normal
MCE	1.18 ± 0.18	1.25 ± 0.29	0.96 ± 0.21*†	1.08 ± 0.23
Slope	1.28 ± 0.34	1.41 ± 0.60	0.98 ± 0.29‡§	1.14 ± 0.31
1/MTT	1.16 ± 0.18	1.19 ± 0.35	0.95 ± 0.27 ¶	1.04 ± 0.19

* $p < 0.002$ pre vs. post; † $p < 0.002$ abnormal vs. normal; ‡ $p < 0.005$ pre vs. post; § $p < 0.06$ abnormal vs. normal; || $p < 0.02$ pre vs. post; ¶ $p < 0.008$ pre vs. post.

to 1 relation. This implies that a given decrease in myocardial blood flow will be represented by a much smaller decrease in MCE. This may be due to the leveling effect of diffusion of Gd-DTPA into the interstitium (36). As the extraction fraction of Gd-DTPA is higher when regional myocardial blood flow is low (37), the difference in Gd-DTPA concentration between hypoperfused and normal myocardium will decrease. Furthermore, despite the use of relative perfusion ratios, regional differences in myocardial vascular volume may still be expected when autoregulation is not ruled out completely. In this case, due to the higher blood volumes, hypoperfused myocardium may thus contain more Gd-DTPA per voxel than normal myocardium, and differences between both areas will be attenuated. Finally, cardiac motion during image acquisition leads to volume averaging of myocardium, which may also decrease the differences in SI between epicardium and endocardium.

Occasional volume averaging of left ventricular cavity and subendocardium may lead to incorrectly high SI in the subendocardium, thus leveling the differences in SI. In addition, in some cases, dark endocardial rims can be observed during the passage of Gd-DTPA through the left ventricular, especially near the septum, which may mimic hypoperfusion. However, these artifacts can be recognized as low signal intensity in the myocardial SI-time curve at the time of high signal intensity in the left ventricular SI-time curve, and in general, artifact-related data points can be rejected for analysis without compromising the curve fit (because there are so many [30–40] data points). Because they are related to high left ventricular signal intensity, artifacts last shorter than true perfusion defects and can thus be discriminated from true perfusion defects by visual analysis as well.

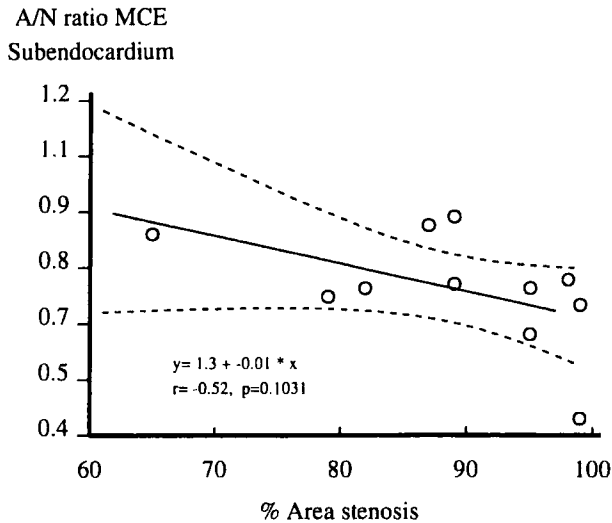
In the presence of a coronary stenosis, the first manifestation of impairment in myocardial perfusion occurs in the subendocardial myocardium (27,28). Initially, perfusion is maintained by the vasodilatory reserve. This regional maldistribution of myocardial perfusion can be

intensified when myocardial autoregulation is ruled out by application of physical or pharmacologic stress. The stress-induced decrease in predominantly subendocardial relative MCE in the patients is likely to reflect this pathophysiology of myocardial hypoperfusion. The differences in A/N ratios of MCE were quite small. Apart from the aforementioned technique-related factors, this may also be caused because these were patients with chronic ischemia who may have developed some degree of collateral circulation. Furthermore, for safety reasons, the dosage of dipyridamole in the patients was lower than in dogs, which may have limited the extent of hypoperfusion. Nevertheless, the presence of the described transmural variations in MCE illustrates the opportunities of MRI to assess relative myocardial perfusion (and abnormalities therein) in sublayers of the myocardium.

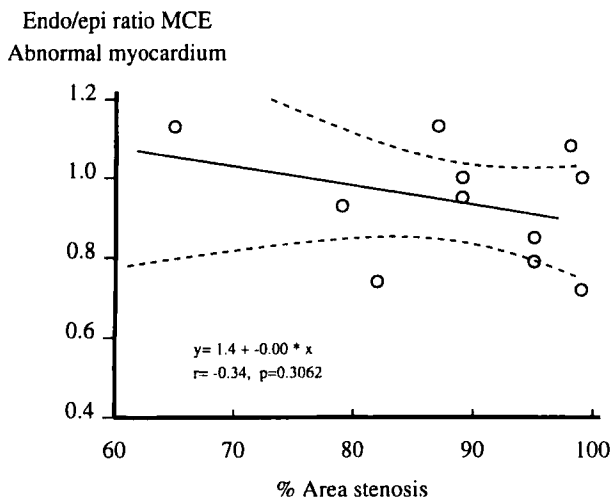
Subendocardial/Subepicardial Ratios

Under physiologic circumstances, the ratio of endocardial to epicardial flow in dogs, averaged throughout the cardiac cycle, is approximately 1.25:1, due to preferential vasodilatation in the subendocardium (27). During stress, this ratio decreases due to the relatively lower perfusion reserve in the subendocardium. In the presence of a subcritical coronary stenosis, however, this ratio may decrease even further due to the dependence of perfusion pressure, which is the lowest in the subendocardial myocardium. Relative MCE as presented in the patients displayed a trend in endo/epi ratios that is in accordance with this pathophysiologic sequence (Fig. 6).

The values of the endo/epi ratios were similar to those in the study of Wilke et al. (31). These data suggest that the transmural redistribution of myocardial perfusion during pharmacologic stress can be evaluated with MRI, including the assessment of abnormalities in this distribution due to the presence of a coronary artery stenosis.



(A)



(B)

Figure 7. Relation between luminal area of the coronary artery stenosis and (A) the subendocardial A/N ratio in abnormal myocardium and (B) the endo/epi ratio in the abnormal myocardium.

Relation with Coronary Angiography

The trend in decrease of subendocardial MCE with increasing coronary stenosis severity suggests that contrast-enhanced MRI may give an indication of the functional severity of a coronary artery stenosis. However, MCE only reflects relative perfusion and may thus not be as useful in patients with multivessel CAD.

The only other noninvasive imaging modality capable of visualizing myocardial perfusion in transmural sublay-

ers is contrast echocardiography (38–40). In the catheterization laboratory, this technique has been shown to delineate differences in transmural perfusion. Present limitations include limited field of view and the necessity of left-sided bolus injection of contrast bubbles that keeps it confined to the catheterization laboratory.

Limitations

In the patient studies, a single short-axis slice was imaged. This saves temporal and spatial resolution but does not allow comprehensive imaging of the whole heart. However, this may be overcome using faster MR sequences. Also, the increase in heart rate may have some effect on the slice position and may thus introduce a small error when comparing the basal and stress state (the rest and stress images were imaged on exactly the same coordinates on the long axis and were anatomically very comparable).

In the patients and in the dogs, all bolus injections of Gd-DTPA were performed by the same investigator to decrease the variability in the rate of injection. Central bolus injection prevents dispersion of the bolus in the peripheral venous system. Nevertheless, the myocardial input function may show variation as considerable dispersion occurs due to anatomic, rheologic, and hemodynamic factors (26,41), including the dimensions and structure of the pulmonary (micro-) circulation, hematocrit, cardiac architecture, ejection fraction, blood pressure, and heart rate. Furthermore, MR signal intensity is subject to variations in heart rate and magnetic field strength. Therefore, when using perfusion parameters MCE and slope (that are dependent on signal intensity), it seems important to focus on A/N and endo/epi ratios resulting from the same injection. However, in our curve fit analysis, 30–40 data points were used and may therefore be not so much dependent on occasional differences in SI due to rhythm or trigger changes.

A more absolute indication of myocardial perfusion may theoretically be expected from perfusion parameter $1/MTT$ (24,26). Derivation of $1/MTT$ requires that the downsloping part of the SI-time curve can be clearly discerned from the recirculation (24). This in turn requires a very compact bolus, for which left-sided bolus injection may be warranted. Previous imaging studies that showed $1/MTT$ to (semi-) quantify myocardial perfusion (38–44) all used left-sided bolus injection, whereas studies that showed a relation with MCE or slope (12–16) used peripheral injection. This may be circumvented by the use of models that incorporate the left ventricular input function (20–22) but is less practical. Recent clinical studies using peripheral injection showed good results using the

peak or maximum contrast enhancement (45,46). This is probably the best approach for clinical practice.

In summary, the results of this study indicate that MRI is capable of at least approximation of the transmural redistribution of myocardial perfusion during pharmacologic stress. Furthermore, perfusion abnormalities due to coronary stenosis were found to be more pronounced in the subendocardium than in the subepicardium. This capability to image differences in myocardial perfusion may contribute to the evaluation of patients with CAD. Improvement in image quality and artifact reduction may enhance the differences between normal and hypoperfused myocardium. With the ongoing developments of fast multislice MR techniques and the forthcoming introduction of new contrast agents, MR perfusion imaging should evolve into a practical clinical tool.

REFERENCES

- White CW, Creighton BW, Doty DB, et al. Does visual assessment of the coronary arteriogram predict the functional importance of a coronary artery stenosis? *N Engl J Med*, 1984; 310:819–824.
- Haronian HL, Remetz MA, Sinusas AJ, Baron J, Miller HI, Cleman MW, Zaret BL and Wackers FTJ. Myocardial risk area defined by technetium-99m Sestamibi imaging during percutaneous transluminal coronary angioplasty: comparison with coronary angiography. *J Am Coll Cardiol*, 1993; 22:1033–1043.
- Strauss HW and Boucher CA. Myocardial perfusion studies: lessons from a decade of clinical use. *Radiology*, 1986; 160:577–584.
- Dunn R, Wolff L, Wagner S and Botvinick E. The inconsistent pattern of thallium defects: a clue to the false positive perfusion scintigram. *Am J Cardiol*, 1981; 48:224–232.
- Bol A, Melin A, Vanoverschelde L, Bauduin T, Vogelaers D, de Pauw M, Michel C, Luxen A, Labar D, Cogneau M, Heijndrickx GR and Wijns W. Direct comparison of 13-N ammonia and 15N water estimates of perfusion with quantification of regional myocardial flow by microspheres. *Circulation*, 1993; 87:512–525.
- Rosen BR, Belliveau JW and Chien D. Perfusion imaging by nuclear magnetic resonance. *Magn Reson Q*, 1989; 5: 263–281
- Higgins CB, Saeed M and Wendland M. Contrast enhancement for the myocardium. *Magn Reson Med*, 1991; 22:347–353.
- Burstein D, Taratuta E and Manning WJ. Factors in myocardial perfusion imaging with ultrafast MRI and Gd-DTPA administration. *Magn Reson Med*, 1991; 20:299–305.
- Frahm J, Merboldt KD, Bruhn H, Gyngell ML, Haenicke W and Chien D. 0.3-Second FLASH MRI of the human heart. *Magn Reson Med*, 1990; 13:150–157.
- Cohen MS and Weiskoff RM. Ultra-fast imaging. *Magn Reson Med*, 1991; 9:1–37.
- Weinmann HJ, Brasch RC, Press WR and Wesbey GE. Characteristics of gadolinium-DTPA complex: a potential NMR contrast agent. *AJR Am J Roentgenol*, 1984; 142:619–624.
- Manning WJ, Atkinson DJ, Grossman W, Paulin S and Edelman RR. First-pass nuclear magnetic resonance imaging studies using gadolinium-DTPA in patients with coronary artery disease. *J Am Coll Cardiol*, 1991; 18: 959–965.
- Atkinson DJ, Burstein D and Edelman RR. First-pass cardiac perfusion: evaluation with ultrafast MR-imaging. *Radiology*, 1990; 174:757–762.
- Schaefer S, Van Tyen R and Saloner D. Evaluation of myocardial perfusion abnormalities with gadolinium-enhanced snapshot MR-imaging in humans. *Radiology*, 1992; 185:795–801.
- Klein MA, Collier BD, Hellman RS and Bamrah VS. Detection of chronic coronary artery disease: Value of pharmacologically stressed, dynamically enhanced turbo-fast low-angle shot MR images. *AJR Am J Roentgenol*, 1993; 161:257–263.
- Matheijssen NAA, Louwerenburg HW, Van Ruge FP, Arens RPJH, Kauer B and Van der Wall EE. Comparison of ultrafast dipyridamole magnetic resonance imaging with dipyridamole SestaMIBI SPECT for detection of perfusion abnormalities in patients with single vessel coronary artery disease: assessment by quantitative model fitting. *Magn Reson Med*, 1996; 35:221–228.
- Keijer JT, van Rossum AC, van Eenige MJ, Bax JJ, Van Eenige MJ, Visser FC, Teule JJ and Visser CA. Magnetic resonance imaging of regional myocardial perfusion in patients with single vessel coronary artery disease: quantitative comparison with ²⁰¹thallium-SPECT and coronary angiography. *J Magn Reson Imaging*, 2000; 11:607–615.
- Keijer JT, Van Rossum AC, Bax JJ, Van Eenige MJ, Visser FC and Visser CA. Measurement of myocardial perfusion and function in myocardial infarction by MRI: comparison with TI-SPECT (abstract). *Eur J Nucl Med*, 1995; 22:766.
- Diesbourg LD, Prato FS, Wisenberg G, Drost DJ, Marshall TP, Carroll SE and O'Neill B. Quantification of myocardial blood flow and extracellular volumes using a bolus injection of Gd-DTPA: kinetic modeling in canine ischemic disease. *Magn Reson Med*, 1992; 23:239–253.
- Wilke N, Kroll K, Merkle H, Wang Y, Ishibashi Y, Xu Y, Zhang J, Jerosch-Herold M, Muehler A, Stillman AE, Bassingthwaite JB, Bache R and Ugurbil K. Regional myocardial blood volume and flow via MR first pass imaging in concert with polylysine-gadolinium-DTPA. *J Magn Res Imaging*, 1995; 5:227–237.
- Wilke N, Jerosch-Herold M, Stillman AE, Kroll K, Tsekos N, Merkle H, Parrish T, Hu X, Wang Y and Bassingthwaite JB. Concepts of myocardial perfusion im-

- aging in magnetic resonance imaging. *Magn Res Q*, 1994; 10:249–286.
22. Kroll K, Wilke N, Jerosch-Herold M, Wang Y, Zhang Y, Bache R and Bassingthwaite JB. Modeling regional myocardial flows from residue functions of an intravascular indicator. *Am J Physiol*, 1996; 40:H1643–H1655.
 23. Bauer WR, Hiller KH, Roder F, Rommel E, Ertl G and Haase A. Magnetization exchange in capillaries by microcirculation affects diffusion-controlled spin-relaxation: a model which describes the effect of perfusion on relaxation enhancement by intravascular contrast agents. *Magn Reson Med*, 1996; 35:43–55.
 24. Meier P and Zierler KL. On the theory of the indicator-dilution method for measurement of blood flow and volume. *J Appl Physiol*, 1954; 6:731–744.
 25. Wilke N, Simm C, Zhang J, Ellermann J, Ya X, Merkle H, Luedemann H, Bache RJ and Ugurbil K. Contrast-enhanced first-pass myocardial perfusion imaging: correlation between myocardial blood flow in dogs at rest and during hyperemia. *Magn Reson Med*, 1993; 29:485–497.
 26. Keijer JT, Van Rossum AC, Van Eenige MJ, Karreman AJ, Hofman MBM and Visser CA. Semiquantitation of regional myocardial blood flow in normal human subjects using first pass magnetic resonance imaging. *Am Heart J*, 1995; 130:893–901.
 27. Braunwald E and Sobel BE. Coronary blood flow and myocardial ischemia. In: Braunwald E, ed. *Heart Disease*. Philadelphia: W.B. Saunders, 1992:1161–1199.
 28. Hoffman JIE. Transmural myocardial perfusion. *Prog Cardiovasc Dis*, 1987; 29:429–464.
 29. Thompson HK, Starmer CF, Whalen RE and McIntosh HD. Indicator transit time considered as a gamma variate. *Circ Res*, 1964; 14:502–515.
 30. Axel L. Cerebral blood flow determination by rapid-sequence computed tomography. *Radiology*, 1980; 137: 679–686
 31. Wilke N, Jerosch-Herold M, Stillman AE, Wang Y, Muehler A, Bache R and Ugurbil K. Myocardial perfusion reserve and transmural perfusion in patients with coronary artery disease (abstract). Proceedings of the 3rd annual meeting ISMRM, 1995, p. 1400.
 32. Jerosch-Herold M and Wilke N. MR perfusion imaging: quantitative assessment of transmural perfusion and collateral flow. *Int J Cardiac Imaging*, 1997; 13:1–14.
 33. Lima JAC, Judd RM, Bazille A, Schulman SP, Atalar E and Zerhouni E. Regional heterogeneity of human myocardial infarcts demonstrated by contrast-enhanced MRI. Potential mechanisms. *Circulation*, 1995; 92:1117–1125.
 34. Crystal GJ, Downey HF and Bashour FA. Small vessel and coronary blood volume during intracoronary adenosine. *Am J Physiol*, 1981; 241:H194–H201.
 35. Wu X, Ewert D, Liu YH and Ritman E. In vivo relation of intramyocardial blood volume to myocardial perfusion. Evidence supporting microvascular site for autoregulation. *Circulation*, 1992; 85:730–737.
 36. Chinard FP, Enns TE and Nolan MF. Indicator-dilution studies with diffusible indicators. *Circ Res*, 1962; 10: 473–490.
 37. Tong CY, Prato F, Wisenberg G, Lee TY, Carroll C, Sandler D and Wills J. Measurement of the extraction efficiency and distribution volume for Gd-DTPA in normal and diseased canine myocardium. *Magn Reson Med*, 1993; 30:337–346.
 38. Cheirif J, Zoghbi WA, Bolli R, O'Neill PG, Hoyt BD and Quinones MA. Assessment of regional perfusion by contrast echocardiography. II. Detection of changes in transmural and subendocardial perfusion during dipyridamole-induced hyperemia in a model of critical stenosis. *J Am Coll Cardiol*, 1989; 14:1555–1565.
 39. Lim YJ, Nanto S, Masuyama T, Kodama K, Ikeda T, Kitabatake A and Kamada T. Visualization of subendocardial myocardial ischemia with myocardial contrast echocardiography in humans. *Circulation*, 1989; 79: 233–244.
 40. Perchet H, Dupouy P, Duval-Moulin AM, Hittinger L, Pelle G, Brun P, Castaigne A, Geschwind H and Dubois-Rande JL. Improvement of subendocardial myocardial perfusion after percutaneous transluminal coronary angioplasty. A myocardial contrast echocardiographic study with correlation between myocardial contrast reserve and Doppler coronary reserve. *Circulation*, 1995; 91:1419–1426.
 41. Nichols KKK, Warner HR and Wood EH. A study of dispersion of an indicator in the circulation. *Ann NY Acad Sci*, 1964; 115:721–737.
 42. Pijls NHJ, Uijen GJH, Hoevelaken A, Arts T, Aengevaeren W, Bos HS, Fast JH, Van Leeuwen KL and Van der Werf T. Mean transit time for the assessment of myocardial perfusion by videodensitometry. *Circulation*, 1990; 81:1331–1340.
 43. Weiss RM, Otoadese EA, Noel MP, DeJong SC and Heery S. Quantitation of absolute regional myocardial perfusion using cine computed tomography. *J Am Coll Cardiol*, 1994; 23:1186–1193.
 44. Porter TA, D'Sa A, Turner C, Jones LA, Minisi AJ, Mohanty PK, Vetrovec GW and Nixon JV. Myocardial contrast echocardiography for the assessment of coronary blood flow reserve: validation in humans. *J Am Coll Cardiol*, 1993; 21:349–355.
 45. Wilke N, Jerosch-Herold M, Wang Y, Huang Y, Christensen BV, Stillman AE, Ugurbil K, McDonald K and Wilson RF. Myocardial perfusion reserve: assessment with multisection quantitative, first pass MR imaging. *Radiology*, 1997; 204:373–384.
 46. Lauerma K, Virtanen K, Sipila LM, Hekali P and Aronen HJ. Multislice MRI in assessment of myocardial perfusion in patients with single vessel proximal left anterior descending coronary artery disease before and after revascularization. *Circulation*, 1997; 96:2859–2867.